ELSEVIER

Journal of Marine Systems 27 (2001) 337–362

JOURNAL OF MARINE SYSTEMS

www.elsevier.nl/locate/jmarsys

One-dimensional modelling of the plankton ecosystem of the north-western Corsican coastal area in relation to meteorological constraints

N. Skliris *, K. Elkalay, A. Goffart, C. Frangoulis, J.H. Hecq

Institut de Physique (B5), Unité d'Ecohydrodynamique, Université de Liège, B4000, Sart Tilman, Belgium

Received 28 June 1999; accepted 26 June 2000

Abstract

In order to study the influence of wind mixing on the spring variability of the plankton production of the north western Corsican coastal area, a one-dimensional (1D), vertical, coupled hydrodynamic/biological model (ECOHYDROMV) is used. A hydrodynamic 1D model of the water column with a *k–l* turbulent closure is applied. The biological model comprises six state variables, representing the plankton ecosystem in the spring period: phytoplankton, copepods, nitrate, ammonium, particulate organic matter of phytoplanktonic origin and particulate organic matter of zooplanktonic origin. The system is influenced by turbulence (expressed by the vertical eddy diffusivity), temperature and irradiance. The model takes into account momentum and heat surface fluxes computed from meteorological data in order to simulate a typical spring atmospheric forcing for the considered area. Results show that primary production vertical structure is characterised by a subsurface maximum which deepens with time and is regulated by the opposite gradients of nitrate concentration and irradiance. Surface plankton productivity is mainly controlled by turbulent vertical transport of nutrients into the mixed layer. The short time scale variability of turbulent mixing generated by the wind appears to be responsible for the plurimodal shape of plankton blooms, observed in the considered area. Furthermore, the model is applied to the study of the spring evolution of the plankton communities off the bay of Calvi (Corsica) for the years 1986 and 1988. In order to initiate and validate the model, time series of hydrological, chemical and biological data have been used. The model reproduces accurately the spring evolution of the phytoplankton biomass measured in situ and illustrates that its strong variability in those years was in close relation to the variability of the wind intensity.

Keywords: coupled hydrodynamic/biological model; north-western Corsican coast; plankton ecosystem; vertical mixing

1. Introduction

The Ligurian current of Atlantic origin, which characterises the surface waters of the north-western Corsican coastal area, determines the oligotrophic character of the local plankton ecosystem. At the end of winter the surface waters of the Ligurian current and of the bay of Calvi (Corsica) present maximum surface concentrations of nitrate, silicate and phosphate of 2.0, 2.0 and 0.2 mmol m^{-3}, respectively (Goffart, 1992). The phytoplankton bloom is usually observed from late February until the end of March (Hecq et al., 1981; Brohée et al., 1989; Goffart,

* Corresponding author. Fax: +32-4-366-2355.
E-mail address: n.skliris@wanadoo.be (N. Skliris).

0924-7963/01/$ - see front matter
PII: S0924-7963(00)00078-6

1992). A chlorophyll maximum of 1–2 mg Chl *a* m^{-3} is measured which is representative of an oligotrophic ecosystem. Copepod biomass, constituting 80–90% of the total mesozooplankton biomass in spring, presents the highest values ($\sim$100 mg dry weight m^{-3}) from late March until the end of April (Dauby, 1985; Brohée et al., 1989). Within the euphotic layer, the vertical distribution of primary producers is determined by the opposite gradients of light and nutrients and by the tendency of phytoplankton cells to sink. The sub-superficial chlorophyll maximum is located at 20 m depth at the beginning of March and exceeds 40 m at the beginning of April (Goffart, 1992). By the end of March the upper layer becomes depleted in nutrients (N03 < 0.2 mmol N m^{-3}). Within the coastal area, the transfer of nutrients from deeper layers is mainly controlled by hydrodynamic processes such as coastal upwellings and turbulent mixing generated by the wind. Some coupled one-dimensional (1D) models, considering a variable vertical turbulent mixing, have demonstrated the regulation of the plankton ecosystem of the Ligurian Sea by the hydrodynamic forcing (Lacroix, 1998; Lacroix and Djenidi, 1992; Tusseau et al., 1997; Levy et al., 1998). Although a close relationship between wind intensity variability and the plurimodal shape of phytoplankton blooms is nearly always observed in the coastal area of Calvi (Hecq et al., 1981; Brohée et al., 1989; Goffart, 1992), the dynamics of that relationship have not been studied by using a modelling approach. The 1D vertical hydrodynamic/biological model elaborated for this study (ECOHYROMV) is adapted to the specificity of the marine system of the north-western Corsican coastal area and is tested for its predictive capacity by using time series of hydrobiological and meteorological data available over several years in this area. Attention is focused on the variability of phytoplankton production in relation to that of vertical nutrient transport into the surface mixed layer.

The coupled hydrodynamic/biological 1D model is based on the assumption of horizontal homogeneity. The station from which data were obtained to initialise and validate the model is located in the western continental shelf off the bay of Calvi (Fig. 1), where bathymetric variations and then upsloping vertical velocities are small. The study area is sufficiently protected from the Liguro-Provençal frontal zone (20 to 25 km from the Corsican coast), where convection occurs. The circulation in this area is determined by the Ligurian Current flowing along the Corsican coast. The mean direction of the measured current at the sampling station is from south-west to north-east, parallel to the coastline (Norro, 1995). This direction often occurs independently of the local meteorological events indicating that upwelling motion is reduced in this area. The examination of data sets over several years shows that a positive vertical nutrient transport in the surface layer is correlated either with north-east wind events

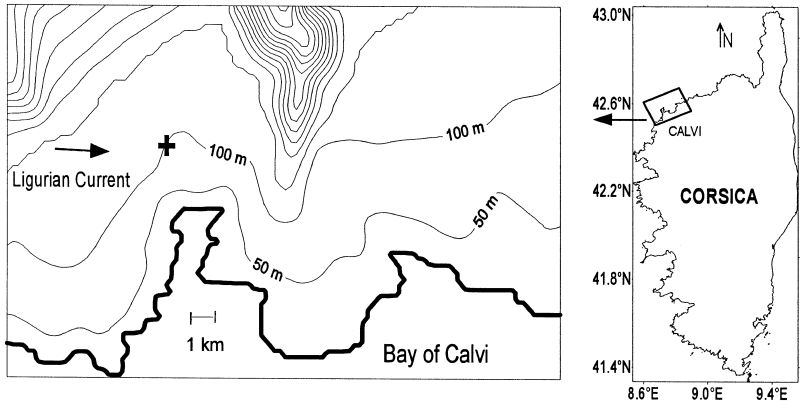

Fig. 1. Bathymetry of the coastal area of Calvi (isobaths every 50 m depth) and location of the station (cross) from which data were obtained to initialise and validate the model.

(which is the optimal direction for upwelling motion in the area) or with south-west wind events (associated with downwelling motion). This fact demonstrates that vertical turbulent motion dominates over vertical advection and thus drives the vertical nutrient transports in the area.

With the aim of simulating a theoretical standard state of the local plankton ecosystem, the model has been first tested with initial conditions and physical forcing constraints corresponding to mean values for this area. Then a sensitivity study is realised for estimating the relative effect of variations in initial conditions, forcing constraints and model parameters on the ecosystem dynamics. Furthermore, additional simulations are performed in order to study the impact of strong wind events on the plankton biomass evolution in the area. In order to make a further validation of this model and to demonstrate the strong correlation between wind intensity and phytoplankton biomass variability, simulations are carried out off the bay of Calvi for the spring period of the years 1986 and 1988, where several secondary phytoplankton blooms have been observed.

2. Data

2.1. Hydrobiological data

Hydrobiological data come from measurements taken in the coastal area of Calvi over several years. Daily surface measurements of hydrological (temperature and salinity) and biological data (chlorophyll *a* (Chl *a*) and mesozooplankton concentrations) are available for the spring period of the years 1979 (Hecq et al., 1981), 1984 (Dauby, 1985), 1986 (Brohée et al., 1989; Goffart, 1992) and 1988 (Goffart, 1992). Daily surface measurements of nutrients concentrations are available for the spring period of the years 1976 (NO_2, NO_3, PO_4) (Bay, 1978) and 1988 (NO_2, NO_3, $SI(OH)_4$) (Goffart, 1992). Furthermore, vertical profiles of temperature (Fig. 2a), salinity, Chl *a* (Fig. 2b) and nutrients (NO_2, NO_3, $SI(OH)_4$) concentrations (10 sampling depths between 0 and 100 m) are available for different periods in spring between 1983 and 1991 (Goffart et al., 1995).

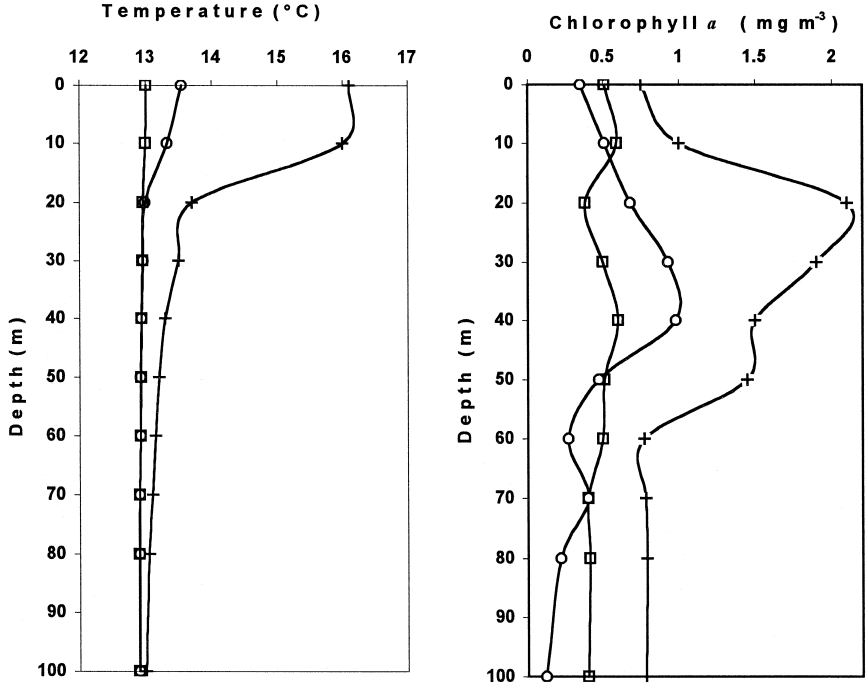

Fig. 2. Vertical profiles of measured variables (bay of Calvi, Corsica). (a) Temperature (°C): 10/03/83 (squares), 03/04/85 (circles) and 11/05/88 (crosses). (b) Chlorophyll *a* concentration (mg m^{-3}): 20/02/84 (squares), 10/03/83 (circles) and the 03/04/85 (crosses).

2.2. Meteorological data

The meteorological data have been provided by the meteorological station of Calvi airport (Meteo, France). Three-hourly measurements of wind (speed and direction), air temperature, relative humidity and cloudiness, are available for the years 1984, 1986 and 1988. Daily global radiation measurements taken in the bay of Calvi are available for the spring period of the years 1979, 1984 (Dauby, 1985) and 1986 (Brohée et al., 1989).

3. Model formulation

The coupled hydrodynamic/biological 1D model is adapted to the spectral window of mesoscale processes (time scale of some hours to some days) where an interaction of resonance appears between hydrodynamic and biological processes (Nihoul and Djenidi, 1991). The mesoscale variability of wind mixing corresponds to the typical duration of a phytoplankton bloom. The hydrodynamic model describes the mixed layer physics. It is driven by momentum and heat fluxes described by functions adjusted to measurements taken in situ. The biological model seeks to reproduce the spring evolution of the principal plankton communities of the study area. The vertical structure of the biological variables is regulated by the mixed layer dynamics in relation to meteorological conditions. The coupling of the two models is carried out by means of the vertical profiles of the eddy diffusivity $\tilde{\lambda}$ and temperature T calculated by the hydrodynamic model and injected at every time step into the biological model. The eddy diffusivity magnitude is a measure of the vertical mixing induced by the wind, which implies a nutrient transport into the mixed layer and thus stimulates the primary production.

3.1. The hydrodynamic model

The hydrodynamic model is based on the GHER 3D, non-linear, primitive equations model (Nihoul and Djenidi, 1987; Nihoul et al., 1989; Beckers, 1991). Since the hypothesis of horizontal homogeneity is assumed, the model is reduced to its vertical dimension (vertical 1D model).

The equations of the 1D model are:

$$\frac{\partial \boldsymbol{u}}{\partial t} + f\boldsymbol{e}_3 \wedge \boldsymbol{u} = \frac{\partial}{\partial x_3}\left(\tilde{\nu}\frac{\partial \boldsymbol{u}}{\partial x_3}\right) \tag{1}$$

$$\frac{\partial T}{\partial x_3} = \frac{\partial}{\partial x_3}\left(\tilde{\lambda}\frac{\partial T}{\partial x_3}\right) \tag{2}$$

$$\frac{\partial S}{\partial t} = \frac{\partial}{\partial x_3}\left(\tilde{\lambda}\frac{\partial S}{\partial x_3}\right) \tag{3}$$

$$\frac{\partial k}{\partial t} = \tilde{\nu}\left|\left|\frac{\partial \boldsymbol{u}}{\partial x_3}\right|\right|^2(1-R_\mathrm{f}) - \varepsilon + \frac{\partial}{\partial x_3}\left(\tilde{\nu}\frac{\partial k}{\partial x_3}\right) \tag{4}$$

$$b(T,S) = -g\frac{\rho-\rho_0}{\rho_0} \tag{5}$$

$$\tilde{\nu} = 0.5l\sqrt{k} \tag{6}$$

$$\tilde{\lambda} = \tilde{\nu}1.1\sqrt{1-R_\mathrm{f}} \tag{7}$$

$$\varepsilon = \frac{k^2}{16\tilde{\nu}} \tag{8}$$

$$l = \kappa z\left(1-\delta\frac{z}{H}\right)(1-R_\mathrm{f}), \qquad 0 \le z \le H \tag{9}$$

with κ the von Karman constant ($=0.4$), z the height above the sea bottom, H the total depth and δ a constant ranging between 0.5 and 1.

$$R_\mathrm{f} = \frac{\tilde{\lambda}\left|\left|\dfrac{\partial b}{\partial x_3}\right|\right|}{\tilde{\nu}\left|\left|\dfrac{\partial \boldsymbol{u}}{\partial x_3}\right|\right|^2} \tag{10}$$

where $\boldsymbol{u}$ is the horizontal velocity vector, $\boldsymbol{e}_3$ is the unit vector along the vertical pointing upwards, f is the Coriolis parameter, g is the acceleration of gravity, b is the buoyancy, T is the temperature, S is the salinity, k is the turbulent kinetic energy, ρ is the local density of the sea water, ρ_0 is a reference Boussinesq density, $\tilde{\nu}$ is the vertical eddy viscosity,

$\tilde{\lambda}$ is the vertical eddy diffusivity, ε is the energy dissipation rate, l is the mixing length and R_f is the flux Richardson number.

A k–l turbulent closure model is used (Nihoul, 1984), consisting of one supplementary evolution equation for the turbulent kinetic energy k (Eq. (4)) and one empirical, algebraic expression for the mixing length l (Eq. (9)). The influence of the stratification is parameterised by the flux Richardson number R_f (Eq. (10)), which measures the relative importance of the production and the inhibition of turbulent kinetic energy.

3.2. The biological model

We use a typical model of the north-western Mediterranean plankton ecosystem which we adapted to the specificity of the plankton ecosystem off the bay of Calvi (Corsica). We choose the dissolved inorganic nitrogen concentration (mmol N m^{-3}) as the unit of the model in order to describe the nitrogen cycle within the ecosystem (Fig. 3). Nitrogen seems to be the most useful nutrient for understanding the inner processes of nutrient flow in the Mediterranean since various fractions exist that represent different aspects of ecosystem processes (Dugdale and Wilkerson, 1988). Phosphorus or silica does not show such fractionation. On another hand, nitrogen appears to be the more limiting element for the phytoplankton growth in the considered area. The phosphorus concentrations are relatively high in this area, in contrast with many Mediterranean regions, due to a continuous phosphate contribution from the seagrass Posidonia oceanica (Bay, 1978; Dauby,

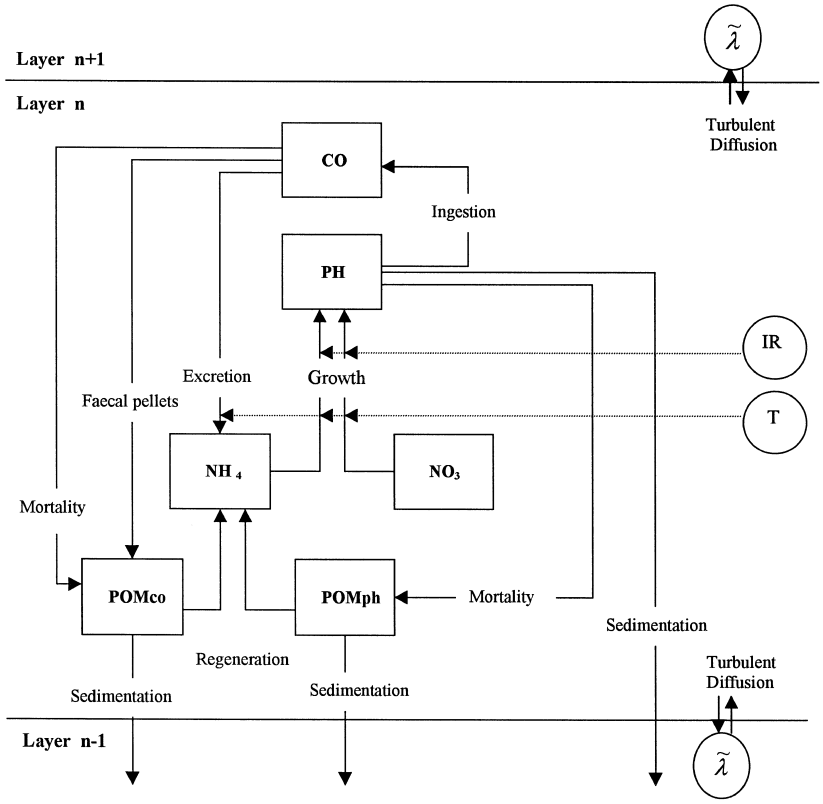

Fig. 3. Block-diagram of the biological model. *State variables*: NO_3: nitrate; NH_4: ammonium; PH: phytoplankton; CO: copepods; POMph: particulate organic matter of phytoplankton origin; POMco: particulate organic matter of zooplankton origin. *Forcing variables*: $\tilde{\lambda}$: vertical eddy diffusivity; T: temperature; IR: irradiance.

1985). The atomic ratio nitrogen/phosphorus presents a maximum value of 10, which is much lower than the Redfield ratio (N/P = 16). In spring the molar ratio nitrate + nitrite/silicate is close to 1 in the sub-superficial waters of the coastal area of Calvi (Goffart, 1992), and then the silica is not considered as a limiting element in the first degree (Jacques and Treguer, 1986).

The model comprises six state variables in order to describe the spring evolution of the plankton ecosystem: phytoplankton (PH), the herbivorous copepods (CO) representing the zooplanktonic compartment; dissolved inorganic nitrogen represented by nitrate (NO_3) and ammonium (NH_4); particulate organic matter of phytoplanktonic origin (POMph) comprising the dead phytoplankton; and particulate organic matter of zooplanktonic origin (POMco) comprising the dead bodies and the faecal pellets of copepods. We consider three forcing variables acting on the system: irradiance IR, temperature T and turbulence (expressed by the eddy diffusivity $\tilde{\lambda}$). The sedimentation of biogenic particles (alive and dead phytoplankton, dead bodies and faecal pellets of copepods) is also considered.

The phytoplankton growth is limited by the nutrients concentration, irradiance and temperature (e.g. Andersen and Nival, 1988). We assume that the nutrient-limitation is controlled by the more limiting nutritive element (e.g. Rhee, 1978; Andersen et al., 1987), which is nitrogen in the study area. We consider that the dissolved inorganic nitrogen consists of nitrate and ammonium in order to distinguish the new and regenerated production (Dugdale and Goering, 1967) and we use the function of Wroblewski (1977) to simulate the ammonium inhibition of the nitrate uptake by the phytoplankton. The functions of limitation by irradiance and temperature are defined by the formula of Peeters and Eilers (1978). They take into account photoinhibition (Platt et al., 1980) and thermoinhibition (Eppley, 1972; Andersen and Nival, 1988), respectively. The ingestion of copepods is represented by the general expression of Ivlev (1955) modified by Parsons et al. (1967). The great difference in the sedimentation velocity between phytoplanktonic and zooplanktonic wastes forces us to distinguish two compartments for the particulate organic matter (e.g. Andersen and Rassoulzadegan, 1991). Sedimentation velocity of faecal pellets and dead bodies of copepods (collected in the study area) was determined in vitro by measuring the time to sink a known distance in a burette filled with filtered seawater allowed to stabilise (e.g. Turner, 1977).

The system of differential equations of the biological model is:

$$\frac{\partial \mathrm{PH}}{\partial t} = (P^{\mathrm{ph}} - M^{\mathrm{ph}})\mathrm{PH} - \mathrm{Grz}^{\mathrm{co}}\mathrm{CO} + \frac{\partial}{\partial z}\left(\tilde{\lambda}\frac{\partial \mathrm{PH}}{\partial z}\right) - W^{\mathrm{ph}}\frac{\partial \mathrm{PH}}{\partial z} \tag{11}$$

$$\frac{\partial \mathrm{NO_3}}{\partial t} = -P^{\mathrm{NO_3}}\mathrm{PH} + \frac{\partial}{\partial z}\left(\tilde{\lambda}\frac{\partial \mathrm{NO_3}}{\partial z}\right) \tag{12}$$

$$\frac{\partial \mathrm{NH_4}}{\partial t} = -P^{\mathrm{NH_4}}\mathrm{PH} + \mathrm{Ex}^{\mathrm{co}}\mathrm{CO} + \mathrm{Rem}(\mathrm{POMph} + \mathrm{POMco}) + \frac{\partial}{\partial z}\left(\tilde{\lambda}\frac{\partial \mathrm{NH_4}}{\partial z}\right) \tag{13}$$

$$\frac{\partial \mathrm{CO}}{\partial t} = (\mathrm{Ass}^{\mathrm{co}}\mathrm{Grz}^{\mathrm{co}} - M^{\mathrm{co}} - \mathrm{Ex}^{\mathrm{co}})\mathrm{CO} + \frac{\partial}{\partial z}\left(\tilde{\lambda}\frac{\partial \mathrm{CO}}{\partial z}\right) \tag{14}$$

$$\frac{\partial \mathrm{POMco}}{\partial t} = (1 - \mathrm{Ass}^{\mathrm{co}}\mathrm{Grz}^{\mathrm{co}} + M^{\mathrm{co}})\mathrm{CO} - \mathrm{Rem}\,\mathrm{POMco} + \frac{\partial}{\partial z}\left(\tilde{\lambda}\frac{\partial \mathrm{POMco}}{\partial z}\right) - W^{\mathrm{mco}}\frac{\partial \mathrm{POMco}}{\partial z} \tag{15}$$

$$\frac{\partial \mathrm{POMph}}{\partial t} = M^{\mathrm{ph}}\,\mathrm{PH} - \mathrm{Rem}\,\mathrm{POMph} + \frac{\partial}{\partial z}\left(\tilde{\lambda}\frac{\partial \mathrm{POMph}}{\partial z}\right) - W^{\mathrm{mph}}\frac{\partial \mathrm{POMph}}{\partial z} \tag{16}$$

The model parameters and the mathematical formulations of the processes are listed in Tables 1 and

Table 1
Processes and parameters of the biological model

Process	Definition	Formulation
Phytoplankton		
Growth		
P^{ph}	Growth rate	$P^{ph} = P^{ph}_{max}$ LIMN LIMIR LIMTE
P^{NO_3}	Growth rate due to NO_3	$P^{NO_3} = P^{ph}_{max}$ $LIMNO_3$ LIMIR LIMTE
P^{NH_4}	Growth rate due to NH_4	$P^{NH_4} = P^{ph}_{max}$ $LIMNH_4$ LIMIR LIMTE
P^{ph}_{max}	Maximum growth rate	
LIMN	Limitation by inorganic nitrogen	$LIMN = LIMNO_3 + LIMNH_4$
$LIMNO_3$	Limitation by NO_3	$LIMNO_3 = e^{-\psi\, NH_4}\,(NO_3/(NO_3 + KNO_3))$
$LIMNH_4$	Limitation by NH_4	$LIMNH_4 = NH_4/(NH_4 + KNH_4)$
KNO_3	Half-saturation constant for NO_3	
KNH_4	Half-saturation constant for NH_4	
ψ	Inhibition constant for NO_3	
LIMIR	Limitation by irradiance	$LIMIR = 2(1 + b_{IR})\,(x_{IR}/(x^2_{IR} + 2\,b_{IR}\,x_{IR} + 1))$
IR_{opt}	Optimal irradiance	
b_{IR}	Shape factor of the photoinhibition curve	$x_{IR} = IR/IR_{opt}$
LIMTE	Limitation by temperature	$LIMTE = 2(1 + b_T)\,(x_T/(x^2_T + 2\,b_T\,x_T + 1))$
T	Temperature	
T_{opt}	Optimal temperature	
T_o	Lower lethal temperature	$x_T = (T - T_o)/(T_{opt} - T_o)$
b_T	Shape factor for the thermoinhibition curve	
Mortality		
M^{ph}	Mortality rate	
N	Nitrogen concentration	pour $N \le N_{min}$ $M^{ph} = M^{ph}_{max}$
N_{min}	Threshold of the mortality curve	
M^{ph}_{max}	Maximum mortality rate	pour $N > N_{min}$ $M^{ph} = a_m/N + M^{ph}_{min}$
M^{ph}_{min}	Minimum mortality rate	
a_m	Shape factor of the mortality curve	
Sedimentation		
W^{ph}	Sedimentation rate	
Copepods		
Ingestion		
Grz^{co}	Ingestion rate	$Grz^{co} = Grz^{co}_{max}(1 - e^{(-k_{iv}(PH - PH_{min}))})$
Grz^{co}_{max}	Maximum ingestion rate	
Ass^{co}	Assimilation coefficient	
k_{iv}	Ivlev's coefficient	
PH_{min}	Threshold concentration for feeding	
Excretion		
Ex^{co}	Excretion rate	
Exo^{co}	Excretion rate at 0°C	$Ex^{co} = Exo^{co}\ b^T_e$
b_e	Shape factor for the excretion curve	
T	Temperature	
Mortality		
M^{co}	Mortality rate	
P.O.M		
Regeneration		
Reg	Regeneration rate	
Sedimentation		
W^{mph}	Sedimentation rate for POMph	
W^{mco}	Sedimentation rate for POMco	

2, respectively. Except from the parameters values determined in vitro or in situ for the study area, the others were chosen following a calibration process, from a range of parameter values used in the pelagic ecosystem models of the Ligurian Sea (Andersen and Nival., 1988; Andersen and Rassoulzadegan, 1991; Andersen et al., 1987; Marcer et al., 1991; Lacroix, 1998; Lacroix and Djenidi, 1992; Levy et al., 1998). The vertical profiles of the temperature and eddy diffusivity are calculated by the hydrodynamic model and they are injected at every time step into the biological model. The temporal evolution of irradiance $IR(t)$ is obtained from the in situ measurements. The photosynthetically active irradiance $IR_{par}(0,t)$ which penetrates the sea surface is calculated by:

$$IR_{par}(0,t) = Par(1 - alb)IR(t) \quad (17)$$

where Par is the percentage of photosynthetically active irradiance and alb is the spring average albedo of the sea surface of the considered area.

The vertical profile of IR_{par} is calculated by:

$$IR_{par}(z,t) = IR_{par}(0,t)e^{-k_e(t)z} \quad (18)$$

where z is the depth and $k_e(t)$ is the light attenuation coefficient considered as independent of depth

Table 2
Numerical values of the biological model parameters

Parameters	Units	Values	Refs.
Phytoplankton			
P_{max}^{ph}	day^{-1}	3.0	Marcer et al., 1991
K_{NO_3}	mmol N m^{-3}	1.0	Marcer et al., 1991
K_{NH_4}	mmol N m^{-3}	0.7	Levy et al., 1998
ψ	(mmol N m^{-3})$^{-1}$	1.5	Fasham et al., 1990
IR_{opt}	W m^{-2}	40	Andersen and Nival, 1988
b_{IR}	w.d.	−0.6	Andersen and Nival, 1988
T_{opt}	°C	16	Andersen and Rassoulzadegan, 1991
T_o	°C	9	Andersen and Rassoulzadegan, 1991
b_T	w.d.	−0.55	Andersen and Rassoulzadegan, 1991
M_{max}^{ph}	day^{-1}	0.1	Andersen et al., 1987
M_{min}^{ph}	day^{-1}	0.03	Andersen et al., 1987
a_m	mmol N m^{-3} day^{-1}	0.035	Andersen et al., 1987
N_{min}	mmol N m^{-3}	0.5	Andersen et al., 1987
W^{ph}	m day^{-1}	0.5	Andersen and Rassoulzadegan, 1991
Copepods			
Grz_{max}^{co}	day^{-1}	0.96	Andersen and Nival, 1988
Ass^{co}	w.d.	0.8	Andersen et al., 1987
k_{iv}	m^3. (mmol N)$^{-1}$	0.5	Marcer et al., 1991
PH_{min}	mmol N m^{-3}	0.02	Marcer et al., 1991
Exo^{co}	day^{-1}	0.0672	Andersen and Nival, 1988
b_e	w.d.	1.025	Andersen and Nival, 1988
M^{co}	day^{-1}	0.04	Marcer et al., 1991
P.O.M			
Rem	day^{-1}	0.1	Andersen and Nival, 1988
W^{mph}	m day^{-1}	1.5	Andersen and Rassoulzadegan, 1991
W^{mco}	m day^{-1}	50	
Irradiance			
$k_{e\,min}$	m^{-1}	0.045	Dauby, 1985
$k_{e\,max}$	m^{-1}	0.12	Dauby, 1985
Par	%	50	Bougis, 1974

and the temporal evolution of which is obtained from the field observations. It presents a maximum in February ($k_e \max \sim 0.12\ m^{-1}$) and a minimum in August ($k_e \min \sim 0.045\ m^{-1}$) (Dauby, 1985).

In order to initiate and validate the model we have to convert the available data of Chl *a* (mg Chl *a* m^{-3}) and copepod concentration (mg dry weight m^{-3}) into terms of nitrogen (mmol N m^{-3}). The phytoplankton concentration is converted by means of the ratio: N Chl $a^{-1} = 9.06$ (mg N mg Chl $a^{-1}) = 0.642$ (mmol N mg Chl a^{-1}) which is a typical value for the Ligurian Sea (Andersen and Nival, 1988). Copepod concentration is converted by means of the mean spring ratio determined for the study area: N dry weight$^{-1} = 0.065$ (mg N mg dry weight$^{-1}) = 0.0046$ (mmol N mg dry weight^{-1}) (Lepoint, personal communication).

3.3. Boundary conditions

3.3.1. Surface boundary conditions

The classical bulk formulas are used to determine the turbulent fluxes at the air–sea interface. The surface boundary conditions for k and $\boldsymbol{u}$ are obtained by expressing the continuity of the momentum and turbulent kinetic energy fluxes (Nihoul, 1984):

$$\tilde{\nu}\frac{\partial \boldsymbol{u}}{\partial x_3}\bigg|_{\text{surf}} = \frac{\rho_a}{\rho_w} C_V |V_{10}| V_{10} \tag{19}$$

$$\tilde{\nu}\frac{\partial k}{\partial x_3}\bigg|_{\text{surf}} = \frac{\rho_{\text{air}}}{\rho_w} C_K |V_{10}|^3 \tag{20}$$

where ρ_a is the specific mass of air at sea level, ρ_w the specific mass of seawater, C_V and C_K are appropriate bulk exchange coefficients and V_{10} is the wind speed measured at 10 m height above the sea surface.

The surface boundary conditions for T are given by (Nihoul, 1984):

$$\tilde{\lambda}\frac{\partial T}{\partial x_3}\bigg|_{\text{surf}} = \frac{F_{\text{net}}}{\rho_{wu} Cp_w} \tag{21}$$

where Cp_w is the specific heat of seawater at constant pressure and F_{net} is the net heat flux at the air–sea surface.

F_{net} is given by:

$$F_{\text{net}} = F_S(1 - \text{alb}) + F_{LW} - F_E + F_H \tag{22}$$

where F_S is the shortwave radiation flux, alb is the sea albedo, F_{LW} is the net upward longwave radiation flux, F_E is the turbulent flux of latent heat and F_H is the turbulent flux of sensible heat.

F_S is obtained from the field observations of daily sea surface irradiance. F_{LW} is approximated by an empirical relationship (Haney, 1971):

$$F_{LW} = 0.985\left\{0.39 - 0.05\left[re_S(T_{10})\right]^{1/2}\right\} \times \left(1 - 0.6 n_c^2\right)\sigma T_S^4 \tag{23}$$

where σ is the Stefan–Boltzman constant, T_S is the sea surface temperature, r is the relative humidity, $e_S(T_{10})$ is the saturation vapour pressure at the air temperature (at 10 m height above the sea surface) and n_c is the fractional cloud cover.

The turbulent fluxes of sensible and latent heat are calculated by bulk formulas:

$$F_H = \rho_a C_H V_{10} C_p^a (T_S - T_{10}) \tag{24}$$

$$F_E = \rho_a C_E V_{10} L\left[q_S(T_S) - q(T_{10})\right] \tag{25}$$

where C_H, C_E are appropriate bulk coefficients, C_p^a is the specific heat of air at constant pressure, L is the latent heat of evaporation, $q_S(T_S)$ is the saturation specific humidity at the sea surface temperature and $q(T_{10})$ is the specific humidity at 10-m height. $q_S(T_S)$ and $q(T_{10})$ are calculated from T_S and T_{10}, respectively, and the tables of thermodynamic properties of water vapour. The quantities needed to estimate the fluxes are obtained from the meteorological data sets.

Since the variations in the sea surface salinity are small in spring for the study area (Brohée et al., 1989), we assume that evaporation and precipitation compensate and thus surface boundary conditions for salinity give zero. For the biological variables we consider that there is no diffusion or sinking across the air–sea interface.

3.3.2. Bottom boundary conditions

We assume a logarithmic bottom layer. The bottom stress is parameterised by (e.g. Blumberg and Melor, 1987):

$$\tilde{\nu}\frac{\partial \boldsymbol{u}}{\partial z}\bigg|_{\text{bottom}} = \left(\frac{0.4}{\ln\dfrac{z(1)}{z_0}}\right)^2 \|\boldsymbol{u}(1)\|\boldsymbol{u}(1) \qquad (26)$$

where $z(1)$ is the height of the centre of the first mesh where the velocity $\boldsymbol{u}(1)$ is calculated and z_0 is the roughness length ($=0.003$).

The bottom boundary conditions for k have been derived by assuming that production balances dissipation of k with neutral stratification:

$$k = 4\tilde{\nu}\left\|\frac{\partial \boldsymbol{u}}{\partial z}\right\| \qquad (27)$$

We assume that there are no heat or salt sources at the sea bottom and thus we consider zero temperature and salinity bottom fluxes. For the biological variables we consider that there is no diffusion at the bottom, but we assume that particulate organic matter sinks into and accumulates in a sediment trap (e.g. Andersen and Nival, 1988).

3.4. Initial conditions

The initial conditions for the fields of temperature T and salinity S are typical data values for the coastal area of Calvi at the beginning of spring (Goffart, 1992; Goffart et al., 1995). The linear vertical profiles are quasi-homogeneous ($T(z=0) = 12.6°\text{C}$–$T(z=100) = 12.4°\text{C}$, $S(z=0) = 38$–$S(z=100) = 37.95$). We consider a typical average velocity of the water column $\boldsymbol{u}_{\text{m}}$ off the bay of Calvi of 10 cm s^{-1} (Norro, 1995), the vertical distribution of which follows a logarithmic profile. We deduce the initial profile of the turbulent kinetic energy by assuming the balance between production and dissipation of energy:

$$k = 0.5^{-4/3} l_{\text{n}}^{4/3}(1-R_{\text{f}})^2\left\|\frac{\partial \boldsymbol{u}}{\partial z}\right\|^{4/3} \qquad (28)$$

The initial conditions (Table 3) for phytoplankton and copepod biomasses and the nutrient concentrations are obtained from the observations in the study area at the beginning of spring (Hecq et al., 1981; Brohée et al., 1989; Goffart, 1992). Since there are no data available for the particulate organic matter concentration, we assume that it constitutes 10% of the alive organic matter (e.g. Marcer et al., 1991). The initial vertical profiles of the biological state variables are homogeneous except for nitrate, which increases linearly from 1 to 3 mmol N m^{-3} between 0 and 100 m.

Table 3
Initial values of the biological state variables, expressed as mmol N m^{-3}

State variables	Initial values
PH	0.22
CO	0.025
NO_3	($z=0$ m): 1 – ($z=100$ m): 3
NH_4	0.2
POMph	0.022
POMco	0.0025

3.5. Discrete model

The differential equations are solved numerically by a standard finite volume technique. A water column of 100-m height is considered. Vertical grid resolution is 2 m and the time step is 10 min. The temporal discretization of the equations is carried out in an explicit way except for the vertical turbulent and sedimentation fluxes, which are treated in an implicit way in order to ensure the stability of the numerical scheme. Space discretisation is implemented by means of a centered-differences scheme.

4. Results and discussion

4.1. Standard run

In order to simulate a standard state of the plankton ecosystem spring evolution, a simulation is performed using initial conditions and physical forcing constraints corresponding to mean values for this area. The temporal evolution of irradiance is described by a sinusoidal function adjusted to the in

situ measurements of daily irradiance taken over several years. Wind speed is taken oscillating sinusoidally around the monthly mean value with a period of 4 days and an amplitude of 2 m s^{-1}, representative of the 4-day mean variation observed in the data sets.

Fig. 4a shows the simulated spring evolution of the vertical profile of temperature. The model reproduces reliably the development of the seasonal thermocline observed in the study area (see Fig. 2a). Until the end of March stratification is week. As spring progresses, the heat flux becomes more and more intense and wind mixing in the upper layer of the euphotic zone induces the establishment of the seasonal thermocline. The spring evolution of eddy diffusivity vertical structure (Fig. 4b) is regulated by wind intensity oscillations and the solar radiation evolution. At the beginning of March the computed mean mixing depth is about 15 m. But as the solar radiation, and then the buoyancy flux, increase with time, eddy diffusivity decreases and the mixed layer becomes thinner (about 10 m at the end of May).

Fig. 5 shows the spring variations of phytoplankton, copepods and nutrients concentrations integrated over 50 m depth. At the beginning of spring the water column is stabilised and primary production is

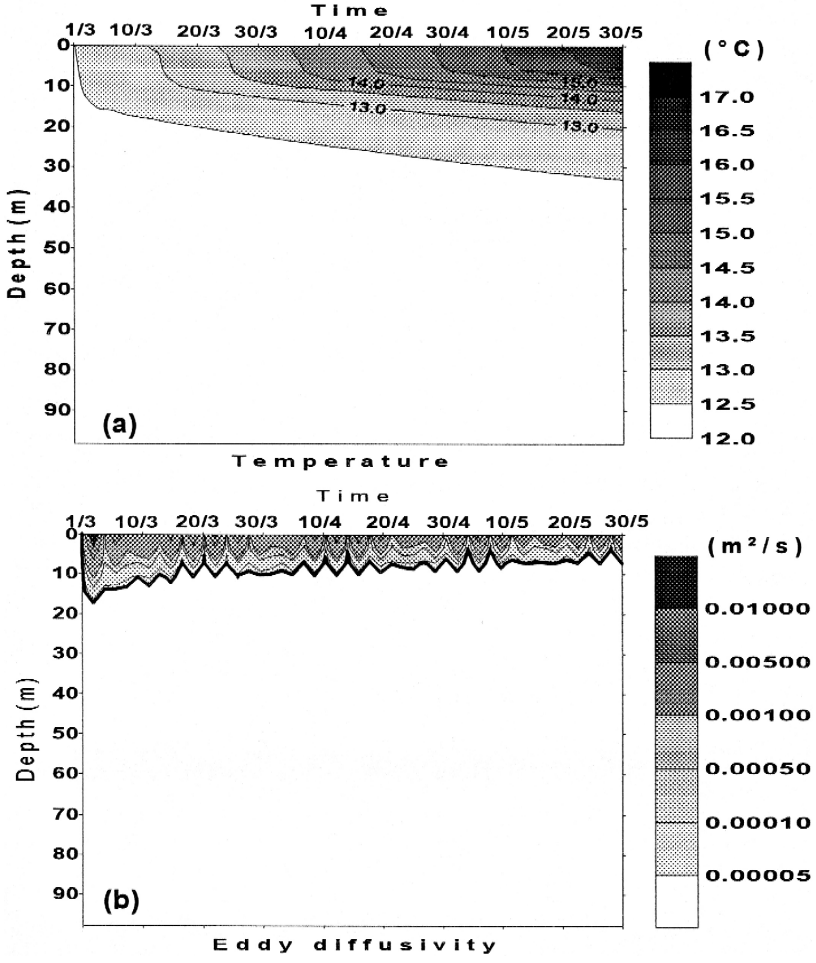

Fig. 4. Spring variations of the vertical structure of: (a) temperature (°C), (b) eddy diffusivity (m^2 s^{-1}). The thick solid line represents the simulated mixed layer depth (using the criteria that $\tilde{\lambda} > 5 \cdot 10^{-5}$ m^2 s^{-1}).

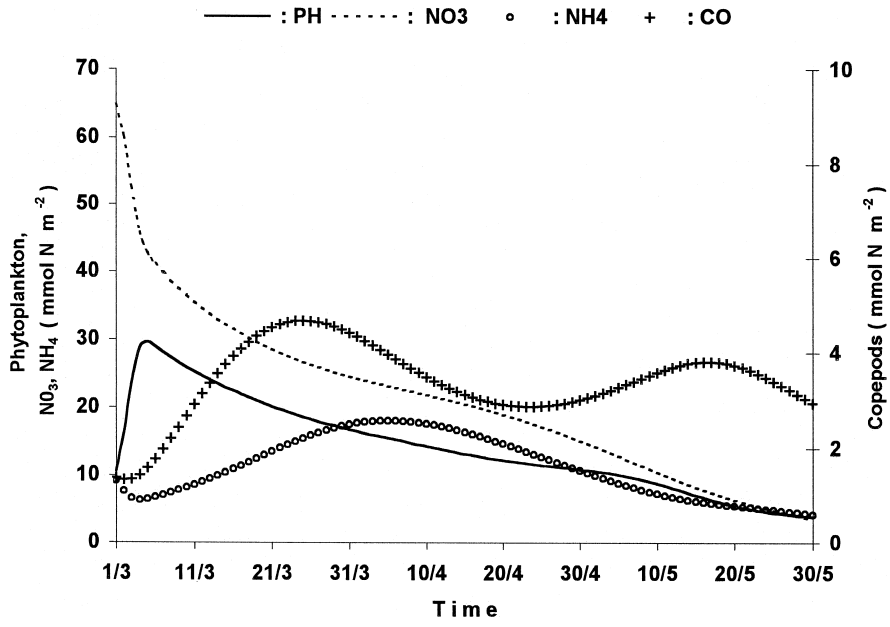

Fig. 5. Spring variations of the integrated biomasses (mmol N m^{-2}) of nitrate (dashed line), ammonium (crosses), phytoplankton (solid line) and copepods (circles) in the upper 50 m.

no longer limited. The euphotic layer depth ($\sim$ 35 m) is significantly deeper than the mixed layer depth ($\sim$ 15 m) allowing phytoplankton cells to grow in light conditions. We simulate the peak of phytoplankton bloom at the first week of March. Phytoplankton consumes rapidly the high amounts of nitrate transported in the upper layer by the intense winter mixing. From the second week of March, nitrate is exhausted in the surface layer. Primary production is sustained by the regeneration process but is not able to compensate losses by grazing and mortality. The spring variation of the simulated depth mean *f*-ratio (ratio between nitrate uptake over total inorganic nitrogen uptake) is typical of the North Western Mediterranean Sea (Minas et al., 1988). It presents high values ($\sim$ 0.9) only during the bloom at the beginning of March due to the high nitrate consumption, but varies between 0.25 and 0.4 at the rest of the season where production is mainly regenerated. Copepod biomass grows when food is available and begins to decrease when the phytoplankton concentrations are too low. The peak of the copepod biomass is simulated at the end of the third week of March. In April the rate of loss of phytoplankton biomass decreases as the surface layer ammonium stock increases and light and temperature conditions become more favourable for photosynthesis. At the end of April, phytoplankton growth almost compensates losses by mortality and grazing allowing copepod biomass to increase slowly and to reach a new peak at mid-May.

Fig. 6 shows the vertical profile of the biological state variables at selected days in the simulation. March 7 and March 25 present the maximum of phytoplankton and of copepod biomass, respectively. The maximum value of the simulated phytoplankton biomass ($\sim$ 1.2 mmol N m^{-3} = 1.87 mg Chl *a* m^{-3}), located at 20 m depth (Fig. 6a), falls in the range of the measured values (1 mg Chl *a* m^{-3}: Hecq et al., 1981 to 2 mg Chl *a* m^{-3}: Goffart, 1992). In the model, the maximum phytoplankton growth occurs when the combined effects of light ant nitrate limitations are minimal. Zooplankton is confined in the upper 50-m layer where primary production is high. The maximum value of copepod biomass (0.27 mmol N m^{-3} $\sim$ 58 mg dry weight m^{-3}) (Fig. 5b), located at 30-m depth, is in the range of the reference data (45 mg dry weight m^{-3} (Hecq et al.,

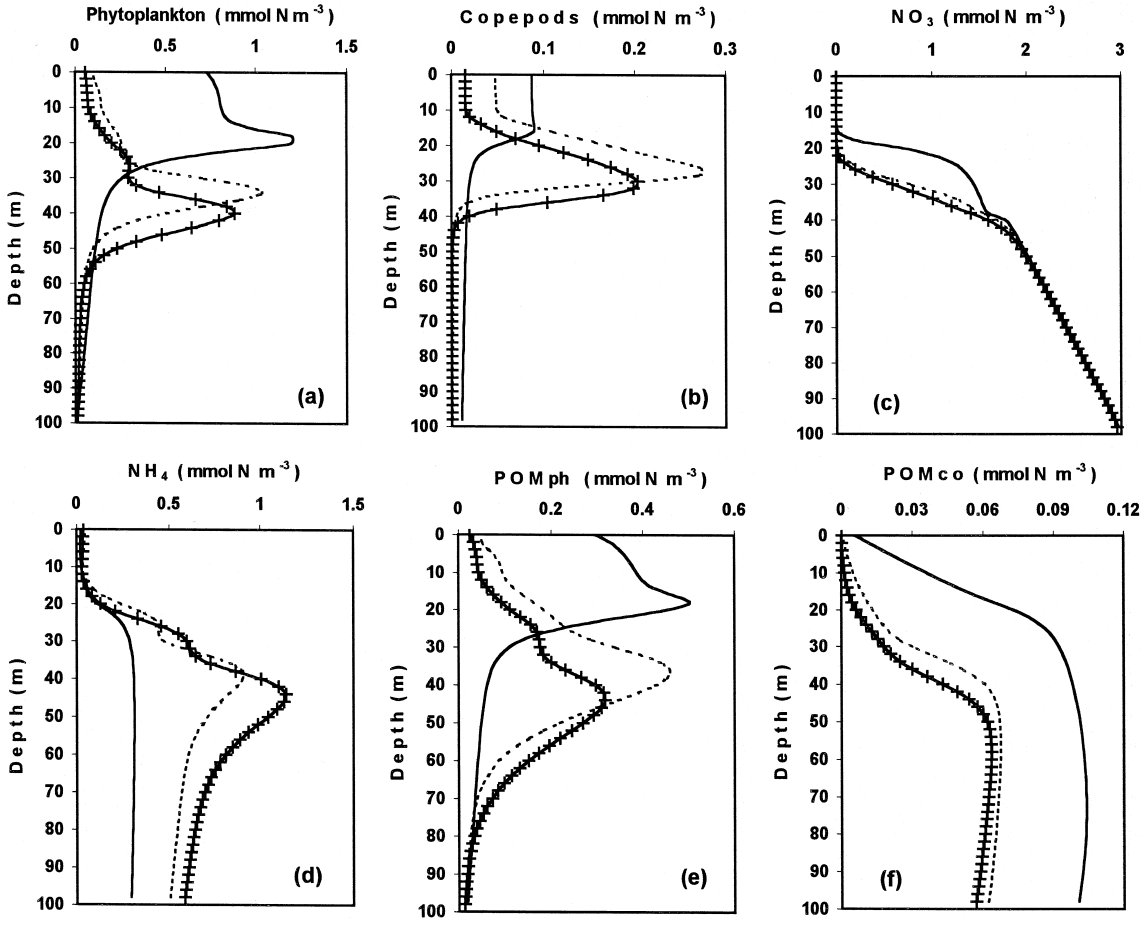

Fig. 6. Vertical profiles of the biological state variables (mmol N m^{-3}) at selected days: March 7 (solid line), March 25 (dashed line) and April 10 (crosses). (a) phytoplankton, (b) copepods, (c) NO_3, (d) NH_4, (e) POMph, (f) POMco.

1981) to 105 mg dry weight m^{-3} (Brohée et al., 1989)). By the end of March, nitrate vertical distribution (Fig. 6c) presents a depleted surface layer (NO_3 < 0.1 mmol N m^{-3}) and a clear nitracline at 30-m depth. Ammonium maximum concentration (Fig. 6d) occurs at 45-m depth just after the copepod peak. The vertical distribution of dead phytoplankton (Fig. 6e) follows that of living phytoplankton. Zooplankton excretion and biodegradation of dead phytoplankton represent the two most significant sources of ammonium in the upper 50-m layer with a spring mean contribution of 55% and 41%, respectively. As a consequence of high sedimentation speed, copepod dead bodies and faecal pellets reach the sea bottom rapidly, and thus they do not significantly contribute to the regenerated production in the surface layer (Fig. 6f).

After the bloom, limitation by nitrate and grazing lead to the depletion of the phytoplankton stock in the surface layer and to the formation of a pronounced subsurface maximum. The propagation of the maximum location (Fig. 7a) follows the depth of the nitracline (Fig. 7b) and is regulated by available light (Fig. 7c). The maximum propagates between the optimum light depth and the base of the euphotic zone. It is located at 30-m depth at mid-March and it exceeds 40 m at the beginning of April, in agreement with the observations (see Fig. 1b). The spring mean downward displacement is about 0.5 m day^{-1}. Until the end of April, the maximum magnitude decreases

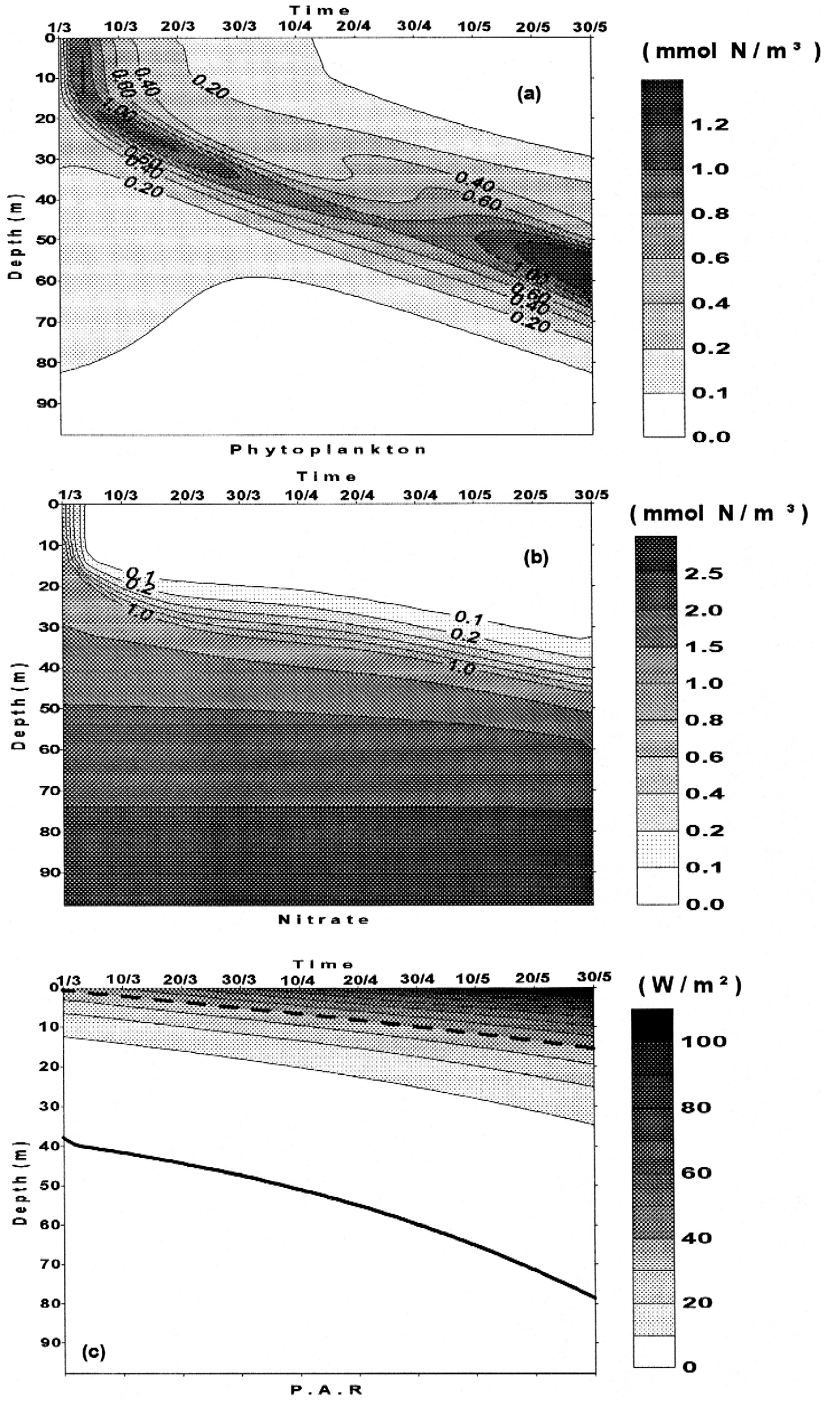

Fig. 7. Spring variations of the vertical structure of: (a) phytoplankton (mmol N m^{-3}), (b) nitrate (mmol N m^{-3}) and (c) photosynthetically active irradiance (W m^{-2}). The thick solid line represents the simulated euphotic layer depth (1% of incident PAR) and the thick dashed line represents the optimum light depth for phytoplankton growth.

with time as a result of decreasing irradiance at the nitracline depth. The temperature of the water column remains quasi-invariable in March when the plankton productivity presents the highest values and thus does not significantly influence the phytoplankton bloom evolution. Turbulent diffusion induces the homogenisation of phytoplankton biomass in a mixed layer of about 10 m. The seasonal thermocline, inhibiting the replenishment of the surface layer with nutrients, is established at mid-April between 10 and 15 m depth and thus does not regulate the subsurface maximum propagation which occurs below this layer. Sedimentation of phytoplankton causes a further deepening and sharpening of the subsurface maximum. The rate of deepening decreases with time due to the rarefaction of light energy and the presence of increasing amounts of nitrate which sustain growth for longer and longer periods of time as the maximum layer deepens. At the beginning of May the subsurface maximum magnitude starts to increase. The rapid increase of solar radiation and the decrease of light attenuation coefficient in that period allow the phytoplankton growth at high depths where nutrients are abundant. At the end of May we simulate a deep phytoplankton maximum formation (at 60 m depth) in agreement with the observations (Goffart et al., 1995). This deep primary production accounts for a large fraction of the total spring production. In late May, 80% of the phytoplankton biomass is confined in a thin layer between 45 and 65 m depth. As a result of high growth rate, the diffused nitrate from the deep layers is rapidly consumed within this maximum layer inhibiting the nitrate replenishment of the upper water column. Moreover, regenerated production mainly occurs within this layer as zooplankton and dead phytoplankton follow phytoplankton biomass time and space evolution. However, the simulated maximum at the end of May (1.1 mmol N m^{-3}) is 30% to 40% higher than the observed values. Furthermore, the model underestimates the nitracline location, which is normally observed 5 to 10 m deeper in that period.

4.2. Sensitivity analysis study

A sensitivity analysis study is realised in order to estimate the relative effect of initial conditions of the state variables, forcing constraints and parameters values variations on the spring evolution of the plankton ecosystem. Variations in initial conditions and forcing constraints (wind intensity and irradiance) are representative of the spring variability observed in the data sets of different years. Variations in model parameters values correspond to the range of values found in the literature for each parameter. Simulations are performed to calculate the spring evolution of the phytoplankton biomass integrated over 50 m and then the mean spring biomass and the maximum biomass values are compared to those of the standard run.

The biological results are the most sensitive to variations of initial conditions of nitrate. Nitrate amount, transported in the upper layer by the intense winter mixing, determines the magnitude of spring primary production in this oligotrophic area. The sensitivity to the initial conditions of the other state variables is much lower. An increase of 25% in the initial nitrate concentration leads to an increase of 8.2% in the mean spring phytoplankton biomass and an increase of 16.3% in its maximum value (Fig. 8a). The variation in the phytoplankton biomass evolution, with respect to the standard run, occurs mostly in early March where nitrate is consumed within a few days. Then the variation is small since the increase of primary production during the bloom is compensated by the loss of phytoplankton biomass due to the increase of grazing pressure.

Fig. 8b shows the changes of phytoplankton biomass evolution due to variations of the monthly average wind speed. Wind mixing deepens the upper mixed layer and thus induces a vertical transport of nutrients into the surface layer where the light conditions are optimal for photosynthesis. An increase of 15% in the monthly average wind speed leads to an increase of 2.1% in the mean spring phytoplankton biomass and an increase of 7.7% in its maximum value. Variations of the surface irradiance ($\pm 5\%$) lead to very small changes in the phytoplankton biomass evolution as a consequence of the small degree of natural variability. An increase of 5% in the surface irradiance leads to an increase of 0.5% in the mean spring phytoplankton biomass and an increase of 1.1% in its maximum value.

Model results are relatively sensitive to the value of parameters included in the formulation of the grazing process and of the photosynthetic produc-

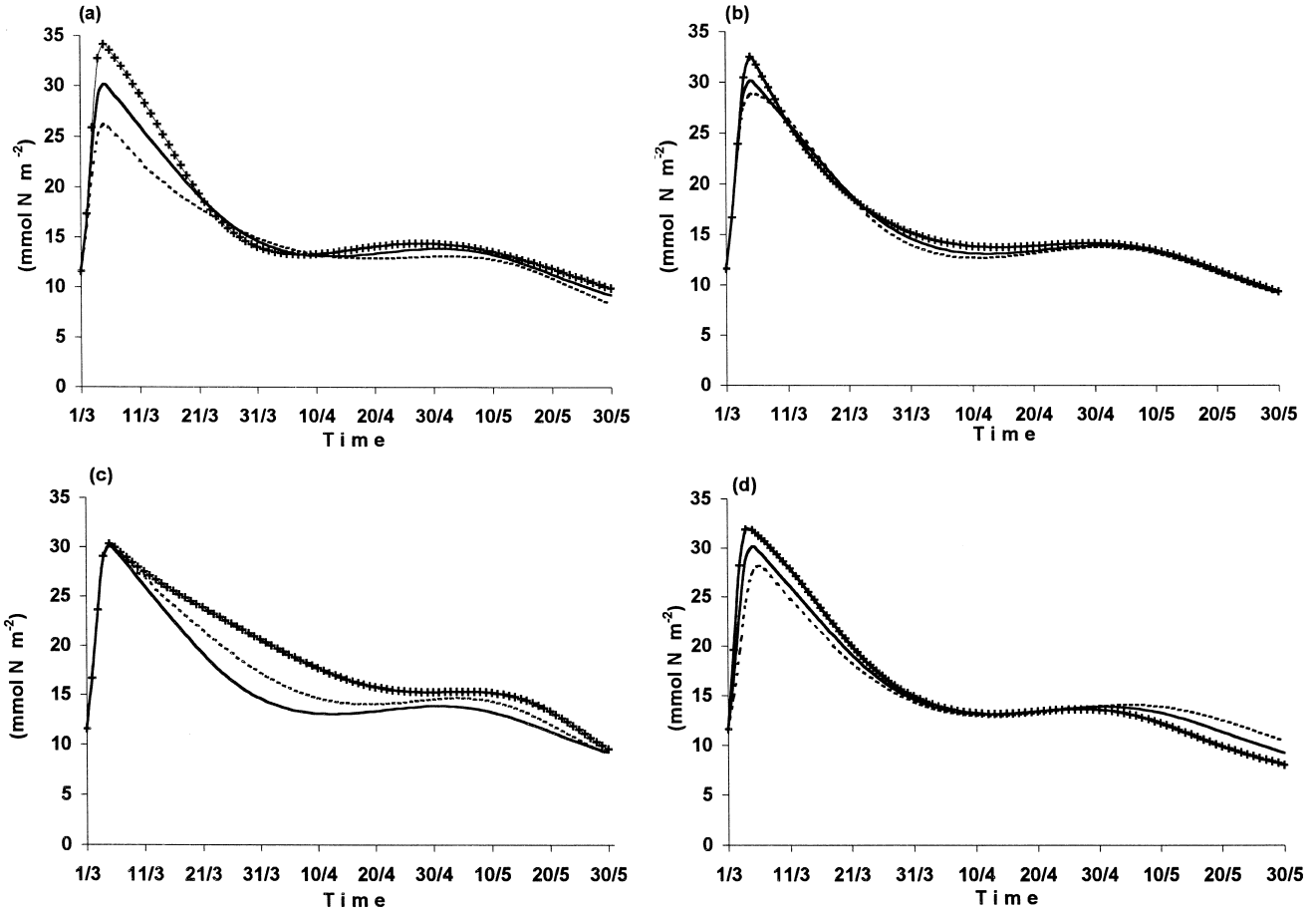

Fig. 8. Influence of initial conditions, forcing constraints and parameters on the evolution of the integrated phytoplankton biomass (mmol N m^{-2}) in the upper 50 m. The solid line represents the standard case. (a) Variation of the initial concentration of nitrate. Initial concentration is 25% higher (crosses) and 25% lower (dashed line) than in the standard case. (b) Variation of the monthly mean wind speed. Wind speed is 20% higher (crosses) and 20% lower (dashed line) than in the standard case. (c) Variation of Ass^{co}: $Ass^{co} = 0.8$ (solid line); $Ass^{co} = 0.7$ (dashed line); $Ass^{co} = 0.9$ (crosses). (d) Variation of T_{opt}: $T_{opt} = 16$°C (solid line); $T_{opt} = 18$°C (dashed line); $T_{opt} = 14$°C (crosses).

tion, indicating that these are the most important biological processes regulating the plankton ecosystem evolution. Although the process formulations and the values of these parameters, chosen from the literature, correspond to populations and similar external conditions of the study area, it is important to determine these values in situ in order to take into account the specificity of the local plankton ecosystem. Fig. 8c and d show the changes in the phytoplankton biomass evolution due to variations in Ass^{co} (assimilation coefficient for copepod ingestion) and T_{opt} (optimal temperature for phytoplankton growth), respectively, parameters to which the model results are the most sensitive. An increase of 12.5% in Ass^{co} leads to a decrease of 4.7% in the mean spring phytoplankton biomass and a decrease of 0.1% in its maximum value. The variation in the phytoplankton biomass evolution, with respect to the standard run, is significant after the phytoplankton bloom when copepod biomass becomes important. An increase of 12.5% in T_{opt} leads to an increase of 1.2% in the mean spring phytoplankton biomass and an increase of 3.8% in its maximum value. Sedimentation velocity of biogenic particles, plankton mortality rates and the parameters related to the regeneration process (copepod excretion, regeneration of particulate organic matter) have a minor influence on the evolution of the plankton ecosystem.

4.3. The ecosystem response to strong wind events

As spring progress the seasonal thermocline develops and imposes a rigorous constraint on the vertical flux of nitrate from deep water. New production leads to the complete nitrate exhaustion in the mixing layer. In the absence of vertical movements related to coastal upwellings or to the instability of the water column (usually, at the beginning of spring the heat budget becomes positive in this area and induces the water column stabilisation), the only possibility of stimulation of the new production in the upper layer is the reinforcement of turbulence generated by the wind. Strong wind events, often occurring in this region, can induce the rapid increase of the mixing depth and the destabilisation of the thermocline. The mean mixing depth and the location of the thermocline observed in situ are 3–4 m deeper than the computed values (standard run). This discrepancy is probably due to the impact of short-term wind variability (time scale of some hours to 1 or 2 days) which is not taken into account in the standard run. The short time scale wind variability yields a chronological sequence of pulsing nutrient enrichment, which can be determinant for primary production in oligotrophic areas (Klein and Coste, 1984). We studied the response of the plankton ecosystem to the speed and duration of a strong wind event. In a simulation a wind event of 12 m s^{-1} during 24 h was introduced, located after the phytoplankton bloom of the beginning of spring (Fig. 9). We observe a new phytoplankton bloom, with a maximum appearing 3 days after the passage of the strong wind event. Prior to the wind event the surface layer is depleted in nitrate (f-ratio ~ 0.25) and the phytoplankton biomass decreases gradually with time. The rate of regenerated NH_4 input in the water column is a slow process, unable to sustain a positive net growth. During the wind event the mixed layer exceeds the depth of the nitracline, which implies an enrichment of the upper layer in nitrate (Fig. 9a and b). The nitrate entrainment from deeper layers starts with a time lag of several hours due to the time and space evolution of turbulent kinetic energy within the mixed layer. Moreover, the phytoplankton biomass remains at moderate levels. Turbulent mixing causes the convergence of one part of the surface plankton into deeper layers where light is more limiting for growth. After the passage of the wind event, the intense mixing stops and phytoplankton, confined by stratification in the upper layer, consumes rapidly the lately transported nitrate (f-ratio ~ 0.8) and a second phytoplankton bloom occurs (Fig. 9c). The new nitrate input magnitude in the upper layer depends on the relative position of the initial nitracline depth and of the mixed layer depth during the wind event. Unlike the regenerated process the new production due to the wind driven nitrate transport leads to a rapid increase of the phytoplankton biomass. The variation in the phytoplankton biomass evolution, with respect to the standard run, is much higher compared to that due to variations in the monthly mean wind speed. The results suggest that the short time scale wind variability has to be taken into account in order to reproduce in more realistic way the plankton ecosystem evolution. The introduction of the wind event

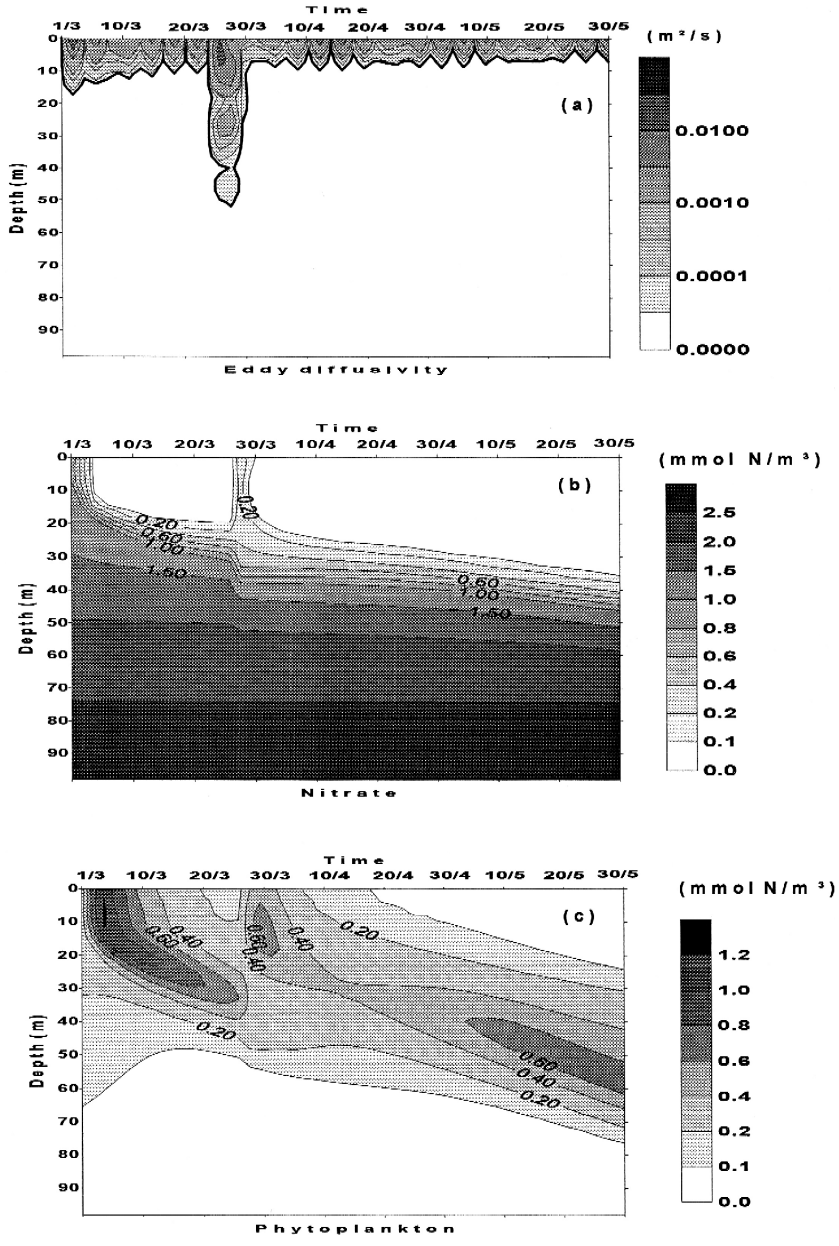

Fig. 9. Spring variations of the vertical structure of variables: (a) eddy diffusivity ($m^2\ s^{-1}$). The thick solid line represents the simulated mixed layer depth (using the criteria that $\tilde{\lambda} > 5 \cdot 10^{-5}\ m^2\ s^{-1}$). (b) Nitrate (mmol N m^{-3}). (c) phytoplankton (mmol N m^{-3}). A wind event of 12 m s^{-1} during 24 h is imposed on March 26.

leads to an increase of about 10% in the spring mean phytoplankton biomass. Furthermore, the passage of the wind event induces a deepening of the nitracline of about 5 m. As a result of decreasing nitrate amount, the deep phytoplankton maximum at the end of May is decreased about 25% which is in accordance with the reference data. Provided that at high depths the growth rate is mainly controlled by light

limitation, the maximum layer position was not altered. By regulating the rate of nitrate consumption, irradiance day to day variations can slow down or accelerate growth but they do not significantly affect the mean new production due to the wind event. A simulation is performed (not shown) where minimum PAR conditions during 48 h succeed the wind event. The phytoplankton peak is simulated 36 h later (with respect to the simulation performed with mean PAR conditions for that period) while the phytoplankton maximum is only decreased about 15%.

Sensitivity analysis simulations (Fig. 10) show that the spring mean phytoplankton biomass level is an increasing function of the speed but also of the duration of the wind event. A wind event during 24 h of a speed of 10, 12 and 14 m s^{-1} leads to an increase in the spring mean phytoplankton biomass

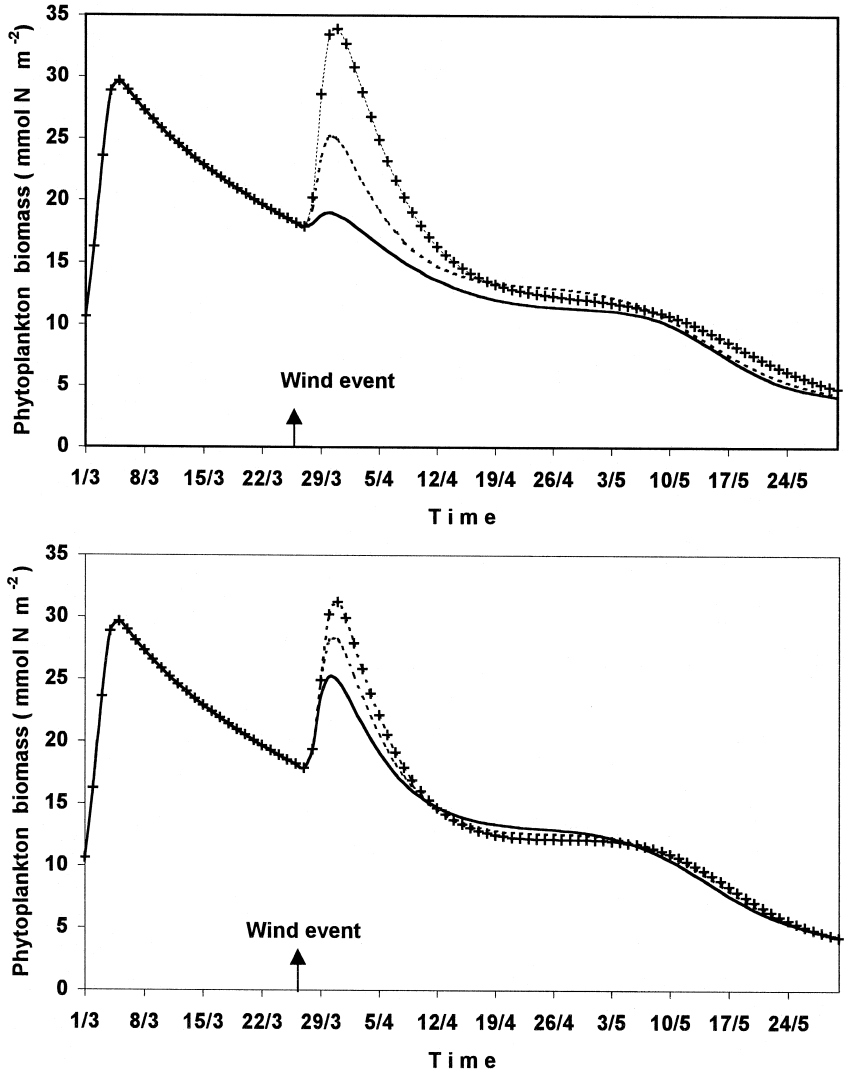

Fig. 10. Spring variations of the integrated phytoplankton biomass (mmol N m^{-2}) in the upper 50 m. (a) A wind event of 10 m s^{-1} (solid line), 12 m s^{-1} (dashed line) and 14 m s^{-1} (crosses) during 24 h is imposed on March 26. (b) A wind event of a speed of 12 m s^{-1} during 24 h (solid line), 36 h (dashed line) and 48 h (crosses) is imposed on March 26.

of 2.9%, 10.2% and 18.1%, respectively (Fig. 10a). A wind event of a speed of 12 m s^{-1} and of a duration of 24, 36 and 48 h, leads to an increase in the spring mean phytoplankton biomass of 10.2%, 12.2% and 14.4%, respectively (Fig. 10b). The more intense or durable the wind is, the higher the biomass maximum will be, but at the same time the latter will appear later because of the dispersion of the plankton during the strong wind event. The model results reveal an ecohydrodynamic resonance which requires the existence of wind events of high speed (>11 m s^{-1}) and of a minimal duration of some hours, or of relatively moderate speed (7–11 m s^{-1}) but of a minimal duration of 1 or 2 days. As the nitracline deepens and stratification becomes stronger with time, further wind events need to be more intense in order to induce a nutrient transport into the upper layer.

4.4. Application to the coastal area of Calvi for spring 1986 and 1988

Very often, it has been suggested that the strong wind events were responsible for the plurimodal aspect of the plankton blooms of the coastal area of Calvi (Hecq et al., 1981; Brohée et al., 1989; Goffart, 1992). In order to make a further validation of our model and to test this hypothesis we have performed simulations for the spring period of the years 1986 (27/02–30/04) and 1988 (28/02–29/04), where several secondary phytoplankton blooms have been observed. Data of surface nutrients and chlorophyll concentrations are available almost every day for both periods and zooplankton surface concentration is available for spring 1986. A real time series of meteorological data (three-hourly measurements) has been used (Brohée et al, 1989; Goffart, 1992) in order to take into account the short time scale variability of heat fluxes and wind stress.

4.4.1. Spring 1986

The model reproduces the plurimodal shape of the phytoplankton biomass evolution observed in situ (Fig. 11a and b). The simulated biomasses are a little higher than the measured ones. One can see, apart from the principal phytoplankton bloom (on March 2), the existence of two secondary phytoplankton peaks (on March 8 and 28) consecutive to a nutrient transport into the surface layer, just after the passage of a strong wind event (Fig. 11c). For both peaks, the new production resulting from this nutrient transport has almost the same magnitude with that of the principal bloom on March 2. For the peak on March 8, it is interesting to note that a wind event of relatively low intensity (on average ~ 7 m s^{-1} during 24 h) is sufficient to make a phytoplankton bloom start again. Since it is the beginning of spring, the water column presents a weak stratification and there are still enough amounts of nutrients in the subsurface layers to stimulate the primary production. Prior to the wind event, surface nitrate concentration is about 0.2 mmol N m^{-3} (Fig. 11c) and the nitracline is located at 20 m depth. Maximum surface concentration after the wind event approaches 0.6 mmol N m^{-3}. The nitrate entrained from the nitracline during the wind event is largely consumed within a single day.

As far as the second peak is concerned, the enhancement of the phytoplankton productivity requires a wind event much more intense (on average ~ 10 m s^{-1} during 24 h) since the subsurface layers are depleted in nitrate (the nitracline is located at 30 m depth) and the grazing pressure is much stronger. Furthermore, the heat flux, which becomes more intense by the end of March, stratifies the upper layer and thus induces the inhibition of turbulence. In addition, the increase of light intensity during this period induces the photoinhibition of phytoplankton growth near the sea surface, in accordance with previous studies in the Ligurian Sea (Andersen and Nival, 1988; Lacroix, 1998). The monthly mean intensity of PAR penetrating the sea surface is increased from 44 W m^{-2} in March to 71 W m^{-2} in April which is much higher than its optimum value for phytoplankton growth (40 W m^{-2}, Andersen and Nival, 1988). As a consequence, the monthly mean value of the light limitation factor (LIMIR) in the sea surface is decreased from 0.72 in March to 0.63 in April. The high wind mixing intensity during the wind event leads to a further delay of phytoplankton peak appearance. In contrast with the first wind event the nitrate is consumed within 3 days. As the season progress, this ecohydrodynamic resonance requires stronger and stronger wind events. Thus, two strong wind events located on April 1 and April 10,

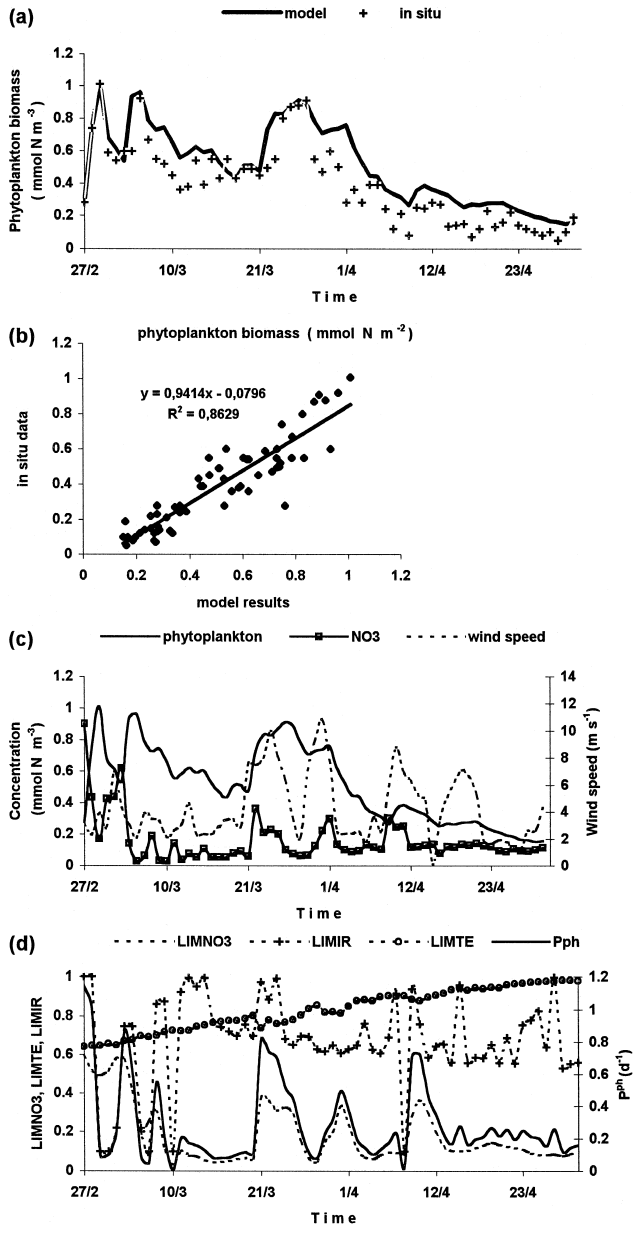

Fig. 11. Application of the model to the coastal area of Calvi in spring 1986 (27/02–30/04/1986). (a) Time variations of surface phytoplankton biomass (mmol N m^{-3}) simulated by the model (solid line) and observed in situ (crosses). (b) Model results vs. in situ data of surface phytoplankton biomass (mmol N m^{-3}). The regression equation is $y = 0.9414 \times - 0.0796$ and the correlation coefficient is $R^2 = 0.8629$. (c) Time variations of surface phytoplankton biomass (mmol N m^{-3}) (solid line), surface nitrate concentration (mmol N m^{-3}) (crosses) and wind speed (m s^{-1}) (dashed line). (d) Time variations of P^{ph} (day^{-1}) (solid line), $LIMNO_3$ (dashed line), LIMIR (crosses) and LIMTE (circles).

respectively, have a minor influence on the plankton biomass evolution.

In order to investigate the relative importance of forcing constraints on phytoplankton biomass evolu-

tion, the variations in growth rate (P^{ph}) and in limitations by nitrate ($LIMNO_3$), light (LIMIR) and temperature (LIMTE) at the sea surface (Fig. 11d), were calculated. Provided that nitrate increases with depth, an increase in surface nitrate concentration (and then in $LIMNO_3$) in this model, is only associated with wind driven turbulent mixing. Results show that growth rate variations mainly follow those of nitrate limitation suggesting that the wind driven nitrate transport regulates phytoplankton biomass variability in this area. Correlation coefficients (R^2) of a linear regression between P^{ph} and $LIMNO_3$, LIMIR, LIMTE are 0.84, 0.25 and 0.05, respectively. Maximum growth rate occurs when a high nitrate transport in the surface layer is combined with optimum light conditions. Temperature limitation factor increases slowly with time as sea surface temperature approaches its optimum value for growth but its day to day variations are too small to affect growth rate variability.

The model simulates the copepod biomass peak around April 10 (Fig. 12), which is in agreement with the in situ measurements, but it is not able to reproduce the variations observed from one day to another. The copepod species determination for that period (Brohée et al., 1989) shows that the various peaks of the total copepod biomass can be associated either with *Centropages typicus* or with *Clausocalanus* sp. peaks. Thus, a part of this variability can be explained by the different physiological characteristics and ingestion rates of the dominant copepod species in the area. Furthermore, the strong variability of each species concentration in the surface layer is not directly correlated with the phytoplankton biomass variability. Copepods developmental stage composition can change dramatically in a period of some weeks. In the bay of Calvi, nauplii constitute 80% of *Clausocalanus* sp. population at the beginning of March while their percentage falls to 10% at the end of April where the population is mainly composed of final stages of copepodites and adults (Dauby, 1985). In each developmental stage, copepods have different nutritional acquirements, mortality and ingestion rates. A model of population dynamics is then necessary to reproduce in a more realistic way the temporal evolution of copepods compartment. On another hand, it has been suggested that vertical migration of copepods, due to food availability and light conditions can be responsible for some of that variability (Dauby, 1985; Brohée et al., 1989). However, at the present time it is difficult to include explicitly the various dominant copepod species as state variables in the model because their migration rates and their population

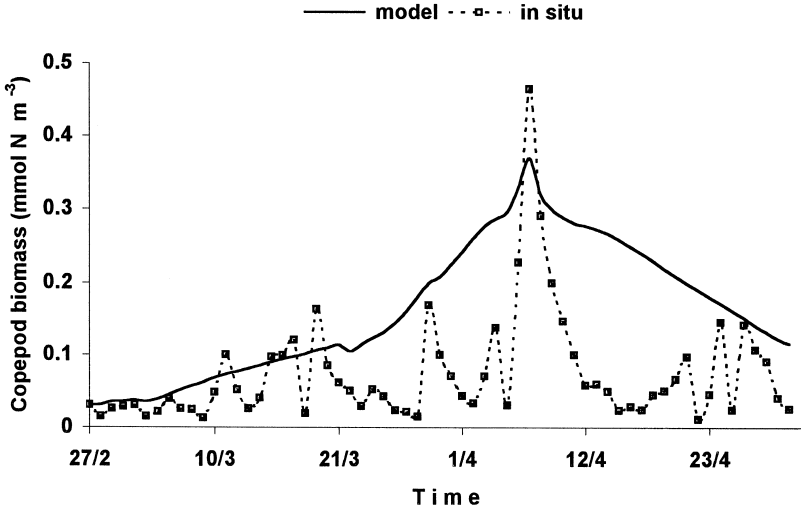

Fig. 12. Time variations of surface copepod biomass (mmol N m^{-3}) simulated by the model (solid line) and observed in situ (coastal area of Calvi, 27/02–30/04/1986).

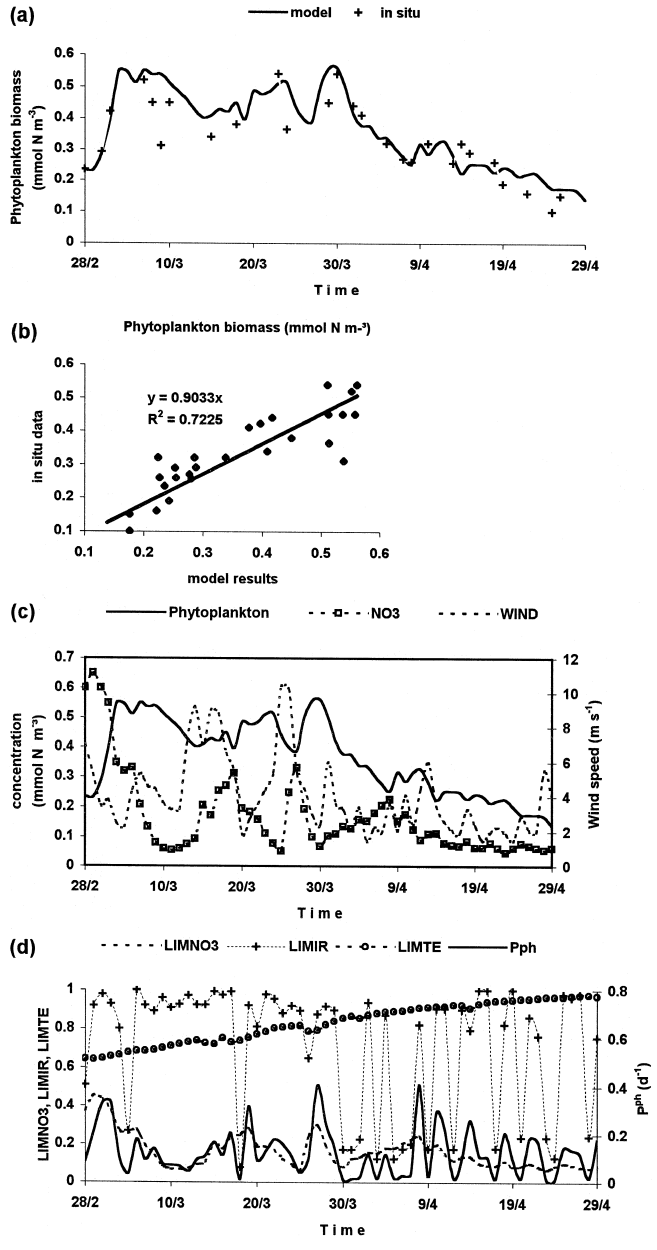

Fig. 13. Application of the model to the coastal area of Calvi in spring 1988 (28/02–29/04/1988). (a) Time variations of surface phytoplankton biomass (mmol N m^{-3}) simulated by the model (solid line) and observed in situ (crosses). (b) Model results vs. in situ data of surface phytoplankton biomass (mmol N m^{-3}). The regression equation is $y = 0.9033 \times$ and the correlation coefficient is $R^2 = 0.7225$. (c) Time variations of surface phytoplankton biomass (mmol N m^{-3}) (solid line), surface nitrate concentration (mmol N m^{-3}) (crosses) and wind speed (m s^{-1}) (dashed line). (d) Time variations of P^{ph} (day^{-1}) (solid line), $LIMNO_3$ (dashed line), LIMIR (crosses) and LIMTE (circles).

dynamics are not sufficiently documented and thus they have to be experimentally determined.

4.4.2. Spring 1988

Like in 1986 simulation, the model reproduces reliably the primary production response to the short-term variability of the forcing (Fig. 13a and b). Two strong wind events are responsible for the phytoplankton peaks on March 24 and March 30 (Fig. 13c). During the first wind event (on average ~ 8.5 m s^{-1} during 96 h) surface nitrate concentration increased from 0.05 to 0.3 mmol N m^{-3}. The phytoplankton peak is simulated 5 days after the passage of the wind event. The delay of peak appearance is associated with relatively low PAR conditions and the persisting mixing of phytoplankton during the wind event. During the second wind event which is stronger but more brief (on average ~ 10.1 m s^{-1} during 48 h) surface nitrate concentration increased again from 0.05 to 0.3 mmol N m^{-3}. However, as a result of better PAR conditions, nitrate is consumed within 2 days and the phytoplankton peak is more pronounced. As in spring 1986, wind driven nitrate transport is the most important factor controlling phytoplankton biomass variability in the surface layer (Fig. 12d). The correlation between growth rate and nitrate limitation is much higher ($R^2 = 0.78$) than that between growth rate and light limitation ($R^2 = 0.28$). It is interesting to note that, unlike spring 1986, phytoplankton biomass remains at low levels. Mean surface primary production for the simulated periods of 1986 and 1988 is 0.141 and 0.075 mg Chl *a* m^{-3} day^{-1}, respectively. This discrepancy can be explained by the difference in the initial nitrate stock of the water column (at the end of February), which is about 30% higher in 1986. Simulated mean surface inorganic nitrogen concentration in March–April 1986 and 1988 is 0.26 and 0.16 mmol N m^{-3}, respectively, while mean light conditions and sea surface temperature evolution are not significantly different. It is possible that the phytoplankton bloom started earlier in 1988 as a consequence of an earlier water column stabilisation and of sufficiently favourable light conditions. However, there are no phytoplankton data available before the simulated period to verify this hypothesis.

The validation of the model for these two years confirms the sensitivity analysis results indicating that nitrate initial conditions as well as wind intensity short-term variability regulate the primary production evolution in this oligotrophic area.

5. Conclusions — perspectives

By means of a coupled 1D hydrodynamic/biological model, we represented the typical spring variations of the vertical structure of the plankton communities of the north-western Corsican coastal area, under the influence of local physical constraints. Apart from the bloom period at the beginning of spring, the regime is oligotrophic and the production mainly regenerated. Primary production vertical structure is characterised by a pronounced subsurface maximum, which deepens with time and is regulated by the opposite gradients of nitrate and of available light. The sensitivity analysis results illustrate that in such oligotrophic coastal area the plankton ecosystem is mainly controlled by turbulent vertical transport of nutrients into the mixed layer. Strong wind events often occurring in this area can strongly stimulate the primary production and restart phytoplankton blooms. The short-term wind intensity variability has to be taken into account in order to reproduce adequately the nutrient transports into the mixed layer as well as the deep chlorophyll maximum formation.

In order to make a further validation of this model, simulations were performed for the coastal area of Calvi in spring 1986 and 1988 by using time series of experimental data. The model proves to be a reliable tool to reproduce the spring evolution of the phytoplankton biomass. The model results enlighten the crucial role played by the wind mixing on the strong variability of the spring primary production of those years.

In our simulations, phytoplankton growth and mortality rates correspond to diatoms physiological characteristics. In the coastal area of Calvi, diatoms dominate the phytoplankton bloom in March (70–80% of the phytoplankton population) while flagellates develop in late spring (Dauby, 1985). Although the model is able to reproduce reasonably well the primary production response to the variability of the forcing, it is important to consider at least two different types of phytoplankton (diatoms and flagellates), characterised by different growth rates and

limitation factors, in order to simulate in a more realistic way the phytoplankton biomass evolution. Furthermore, three suggestions are made in order to improve model representation of copepod biomass variability: distinguishing the dominant copepod species of the area as state variables in the model, determining their migration rates and introducing a sub-model of population dynamics.

References

Andersen, V., Nival, P., 1988. Modèle d'écosystème pélagique des eaux côtières de la mer Ligure. Oceanol. Acta, Vol. sp., pp. 211–217.

Andersen, V., Rassoulzadegan, F., 1991. Modèle vertical de l'écosystème pélagique marin. Réseau microbien et sédimentation des particules biogéniques. J. Rech. Océanogr. 16, 16–22.

Andersen, V., Nival, P., Harris, R.P., 1987. Modelling of a planktonic ecosystem in an enclosed water column. J. Mar. Biol. Assoc. UK 67, 407–430.

Bay, D., 1978. Etude in situ de la production primaire d'un herbier de posidonies de la baie de Calvi, Corse. PhD Thesis, Univ. Liège, Belgium.

Beckers, J.M., 1991. Application of the GHER 3D general circulation model to the Western Mediterranean. J. Mar. Syst. 1, 315–332.

Blumberg, A.F., Melor, G.L., 1987. A description of a three-dimensional coastal ocean circulation model. In: Heaps (Ed.), Three Dimensional Coastal Ocean Models. American Geophysical Union, pp. 1–16.

Bougis, P., 1974. Ecologie du Plancton Marin, Collection d'écologie, vol. 2. Masson, 196 pp.

Brohée, M., Goffart, A., Frankignoulle, M., Henri, V., Mouchet, A., Hecq, J.H., 1989. Variations printanières des communautés planctoniques en baie de Calvi (Corse) en relation avec les contraintes physiques locales. Cah. Biol. Mar. 30, 321–328.

Dauby, P., 1985. Dynamique et productivité de l'écosystème planctonique du golfe de Calvi–Corse, PhD Thesis, Univ. Liège, Belgium, 291 pp.

Dugdale, R.C., Goering, J.J., 1967. Uptake of new and regenerated forms of nitrogen in primary productivity. Limnol. Oceanogr. 12, 179–184.

Dugdale, R.C., Wilkerson, F.P., 1988. Nutrient sources and primary production in the Eastern Mediterranean. Oceanol. Acta, Vol. sp., pp. 179–184.

Eppley, R.W., 1972. Temperature and phytoplankton growth in the sea. Fish. Bull. 70, 1063–1085.

Goffart, A., 1992. Influence des contraintes hydrodynamiques sur la structure des communautés phytoplanctoniques du bassin Liguro-Provençal (secteur Corse), PhD Thesis, Univ. Liège, 163 pp.

Goffart, A., Hecq, J.H., Prieur, L., 1995. Contrôle du phytoplancton du bassin Ligure par le front liguro-provençal (secteur Corse). Oceanol. Acta 18 (3), 328–342.

Fasham, M.J.R., Ducklow, H.W., McKelvie, S.M., 1990. A nitrogen–based model of plankton dynamics in the oceanic mixed layer. J. Mar. Res. 48, 591–639.

Haney, R.L., 1971. Surface thermal boundary condition for ocean circulation models. J. Phys. Oceanogr. 1 (4), 241–248.

Hecq, J.H., Gaspar, A., Dauby, P., 1981. Caractéristiques écologiques et biochimiques de l'écosystème planctonique en baie de Calvi (Corse). Bull. Soc. R. Sci. Liège 50^{e} année (11–12), 440–445.

Ivlev, V.S., 1955. Experimental Ecology of the Feeding of Fishes. Yale Univ. Press (1961), New Haren, 302 pp.

Jacques, G., Treguer, P., 1986. Ecosystèmes Pélagiques Marins, Collection d'écologie. Masson, 243 pp.

Klein, P., Coste, B., 1984. Effects of wind stress variability on nutrient transport into the mixed layer. Deep-Sea Res. 31, 21–37.

Lacroix, G., 1998. Simulation de l'écosystème pélagique de la mer Ligure à l'aide d'un modèle unidimensionnel. Etude du bilan de matière et de la variabilité saisonnière, interannuelle et spatiale. PhD Thesis, Univ. Liège, Belgium and, Univ. Pierre and Marie Curie, Paris VI, France, 256 pp.

Lacroix, G., Djenidi, S., 1992. Extending the GHER model to the modelling of ecosystemes in western mediterranean coastal zones: Results from an exploratory study. Water Pollution Research, Third EROS 2000 workshop on Research in the North-Western Mediterranean sea, Commission of the European Communities, Texel, October, 1991. pp. 89–104.

Levy, M., Memery, L., Andre, J.M., 1998. Simulation of primary production and export fluxes in the Northwestern Mediterranean Sea. J. Mar. Res. 56, 197–238.

Marcer, R., Fraunie, P., Dekeyser, I., Andersen, V., 1991. Modélisation numérique d'un couplage physico-biologique en milieu côtier. Oceanol. Acta 11, Vol. sp., pp. 71–79.

Minas, H.J., Minas, M., Coste, B., Gostan, J., Nival, P., Bonin, M.C., 1988. Production de base et de recyclage: une revue de la problématique en Méditerranée Nord-Occidentale. Oceanol. Acta 9, 155–162.

Nihoul, J.C.J., 1984. A three-dimensional general marine circulation model in a remote sensing perspective. Ann. Geoph. 2 (4), 433–442.

Nihoul, J.C.J., Djenidi, S., 1987. Perspective in three-dimensional modeling of the marine System. In: Nihoul, J.C.J., Jamart, B. (Eds.), Three-Dimensional Models of Marine and Estuarine Dynamics. Elsevier, Amsterdam, pp. 1–34.

Nihoul, J.C.J., Djenidi, S., 1991. Hierarchy and scales in marine Ecohydrodynamics. Earth Sci. Rev. 31, 255–277.

Nihoul, J.C.J., Deleersijder, E., Djenidi, S., 1989. Modelling the general circulation of shelf seas by 3D k–e models. Earth Sci. Rev. 26, 163–189.

Norro, A., 1995. Etude pluridisciplinaire d'un milieu côtier. Approches experimentale et de modélisation de la baie de Calvi (Corse), PhD Thesis, Univ. Liège, Belgium, 239 pp.

Parsons, T.R., Lebrasseur, R.J., Fulton, J.D., 1967. Some observations on the dependance of zooplankton grazing on cell size and concentration of phytoplankton blooms. J. Oceanogr. Soc. Jpn. 23, 10–17.

Peeters, J.H.H., Eilers, P., 1978. The relationship between light

intensity and photosynthesis in natural assemblages. A simple mathematical model. Hydrobiol. Bull. 12, 134–136.
Platt, T., Gallegos, C.L., Harrison, W.G., 1980. Photoinhibition of photosynthesis in natural assemblages of marine phytoplankton. J. Mar. Res. 38, 687–701.
Rhee, G.Y., 1978. Effects of N:P atomic ratios and nitrate limitation on algal growth cell composition, and nitrate uptake. Limnol. Oceanogr. 23, 10–25.
Turner, J.T., 1977. Sinking rates of fecal pellets from the marine copepod Pontella meadii. Mar. Biol. 40, 249–259.
Tusseau, M.H., Lancelot, C., Martin, J.M., Tassin, B., 1997. 1D coupled physical–biological model of the northwestern Mediterranean Sea. Deep-Sea Res. II 44 (3–4), 851–880.
Wroblewski, J., 1977. A model of phytoplankton plume formation during variable Oregon upwelling. J. Mar. Res. 35, 357–394.